Renewable Energy 164 (2021) 978–989

Contents lists available at ScienceDirect

Renewable Energy

journal homepage: www.elsevier.com/locate/renene

A numerical investigation to analyze effect of turbulence and ground clearance on the performance of a roof top vertical–axis wind turbine

M. Salman Siddiqui [a, *], Muhammad Hamza Khalid [b], Rizwan Zahoor [c], Fahad Sarfraz Butt [d], Muhammed Saeed [e], Abdul Waheed Badar [d]

[a] Department of Architecture & Technology, Norwegian University of Science & Technology, Trondheim, Norway
[b] Department of Mathematical Science, Norwegian University of Science & Technology, Trondheim, Norway
[c] Faculty of Mechanical Engineering, University of Ljubljana Askerceva, Ljubljana, Slovenia
[d] Department of Mechanical Engineering, HITEC University, Taxila, Pakistan
[e] Mechanical Engineering Department, Khalifa University of Science and Technology, Sas Al Nakhl Campus, Abu Dhabi, United Arab Emirates

ARTICLE INFO

Article history:
Received 9 September 2019
Received in revised form
20 August 2020
Accepted 5 October 2020
Available online 16 October 2020

Keywords:
Vertical-axis wind turbine
Turbulence intensity
Ground clearance
High fidelity simulations
Sliding mesh interface

ABSTRACT

Recent attempts to discover energy–efficient and cost–effective power generation systems unleash tremendous capabilities of urban rooftops vertical–axis wind turbines (VAWT). Their advantages of Omni–directionality, low noise and less maintenance cost allow direct integration to urban neighborhood having unstable wind conditions. Despite continuous effort to investigate performance under a range of operating conditions, aspects such as Turbulent Intensity (*TI*) and ground clearance remain relatively less explored. Such effects originate either due to sharp topographical variations or placement of the turbine blades in proximity to the ground. In the present work, we perform a parametric study to quantify the performance of VAWT under various levels of *TI* and ground clearance. We conduct high fidelity Computational Fluid Dynamics (CFD) simulations using ANSYS Fluent and $k-\varepsilon$ turbulence model. The H-type VAWT is employed having rated power of 1.5 *kW*, diameter (D)of 2.5 *m*chord length (c) of 0.2 *m* and operates at prescribed wind speed (U_0)of 12.0 *m*/sand Tip Speed Ratio (*TSR*) of 1.5–4.5. We determine the performance of turbine under four levels of *TI* i.e., 0%, 5%, 15%25%at five ground clearance levels of $1.0c, 2.5c, 4.0c, 7.5c$and $10.0c$. The results show a performance loss of 30.10%, 20.65%, 10.65% at turbine clearance heights of $1.0c, 2.5c$, $4.0c$ respectively. The height of $7.5c$ yield higher and more consistent performance under given operating conditions. The results for induced turbulence identify a decrease in the performance up to 45.42% corresponding to 25% *TI* level.

1. Introduction

The contradictions between the increasing depletion of fossil fuels and rising demands of power have started to become acute [1]. It has sparked an urgency among energy activists to look for alternative energy resources to meet future energy requirements. A recent survey [2] reports 35% increase in primary energy consumption by 2040 while predicting a considerable decline in oil production at the same time. Energy production through conventional thermal power plants leaves environmental footprints; despite this fact, they remain principal contributors to total world power generation [2–4]. Renewable energy as clean, abundant, and sustainable, is expected to grow and dominate the future energy market. To this end, energy harvesting through wind has shown tremendous potential and future installations are expected to grow at the rate of 5% each year [5].

Depending on wind conditions, large wind power plants in the past were either deployed at remote locations on land or along the coast [6–8]. With the recent success of the floating farm concept, the wind energy community is more inclined towards offshore installations [1,9–11]. Regarding small scale applications, strong evidence is available towards utilization of small scale wind turbines in an urban context where wind flow structure is complex and is ascribed by high directional variability, large skew angles, and high turbulent content. Although the aforementioned conditions cause power degradation, yet rooftop wind turbines remain an integral component of net-zero buildings and neighborhoods.

In comparison to Horizontal Axis Wind Turbines (HAWT),

* Corresponding author.
E-mail address: muhammad.siddiqui@ntnu.no (M.S. Siddiqui).

https://doi.org/10.1016/j.renene.2020.10.022

Straight Bladed Vertical–Axis Wind Turbines (SB–VAWT) exhibit several advantageous features when placed on rooftops of high rise buildings. They are omnidirectional, offer less installation/maintenance costs, produce lower noise emissions, and perform well under highly turbulent conditions [12–14] – making them ideal for urban environments. Common VAWTs design is segregated on drag (Savonius) and lift (Darrieus) type concepts. Unlike drag based Savonius type VAWT, lift based H–rotor Darrieus VAWT [15] exhibits advantageous of self start, high efficiency under low wind speeds and higher Tip Speed Ratios (*TSR*s).

Previous studies on energy harvesting in urban environments suggest a performance deterioration of turbines mounted on the rooftop of high rise buildings in connection to high turbulence, large circulation zones and uneven airflow distribution [3,16,17]. One of the prime causes includes disproportionate placement in connection to roof profiling [18–22], building spacings [23], or channeling effects [23–25]. The optimal design of VAWTs requires a comprehensive analysis of the geometric and operational parameters for maximum power harvesting. Significant research efforts have been placed to investigate the effect of geometric parameters, such as airfoil shape [26,27], number of blades [28,29], blade pitch angle [30], turbine shaft [31]. Another enormous potential of Darrieus SB–VAWT performance in an urban environment is related to identifying optimized ground clearance and *TSR* that provides minimal shearing effect between rotating blades and a flat surface at which the turbine is mounted. This shearing phenomenon often becomes a bottleneck for the turbine to unleash its full potential [32]. Mounting of the turbine at a certain height is directly associated with the costs of tower design, manufacture, and installation. Few scientific studies and industry standards suggest a minimum tower height of 2.5 times nearby building or trees in an urban environment [33,34]. A CFD study conducted by Heath et al. [18] suggest a hub height of at least 50% above building height is required to capture wind that is not significantly affected by the surrounding buildings. However, as reported in Ref. [35,36], even a 10 times height increase compared to nearby obstruction, the average wind speed is reported to decrease, followed by a 6% increase in turbulence and 17% power drop compared to undisturbed upstream conditions.

Turbulence generated from the topographical factors disrupts the smooth airflow over the turbines blade resulting in sharp wind speed and direction changes. While numerical and experimental studies have been performed at fixed turbulence levels, in an urban environment the freestream turbulence intensity varies widely [37–44]. Studies suggest a *TI* variation of 0%–30% in an urban neighborhood with a strong influence on the overall performance of rooftop wind turbines. Replicating such flows in experimental facilities is difficult, owing to the limitations and difficulty in recreating the urban environment with highly turbulent flow. Molina et al. [40] performed experimental analysis to study the effect turbulence on the performance of VAWT using parametric variation on grid sizes up to 15% *TI*. At low *TSR*, the transition from 0.5% to 15% increases the power coefficient while the converse trend is observed at Reynolds number larger than 400,000. Given the fact that *TI* can easily exceed 30% in an urban environment. Lee et al. [41] investigates the case with more than 30% *TI* and report an increase in power of VAWT at high *TI* and lower wind speed while showing adverse effect at higher wind speed. A study by Rezaeiha et al. [42] shows an improvement in turbine performance in the dynamic stall, with an overall deteriorated optimal performance for *TI* level greater than 5%. Similarly, a study on the effect of *TI* by Siddiqui et al. [43] reports a 23%–42% drop in performance when the *TI* is increased to 25%.

The scientific literature, as discussed above, identify a trivial need to analyze the combined effect of *TI*, ground clearance, and *TSR* to draw plausible conclusions of performance deterioration for rooftop turbines. Given economic limitations to perform an experimental investigation, a high fidelity CFD investigation deemed sufficient for present work. Such parametric investigations highlight the benefits of maintaining optimal *TSR* in contrast to ground clearance and *TI* for maximum power harvesting. To the best of author's knowledge, such investigation has not been performed in the past on a single turbine model. Therefore, the present study investigates the influence of the aforementioned gaps for a Darrieus type SB–VAWT and address the following trivial questions. (a) How does ground clearance effect Darrieus SB–VAWT performance, in terms of *TSR*, torque ripple and power coefficient (C_p). (b) What is the effect of *TI* variation in an urban neighborhood on the power output of SB–VAWT. (c) To investigate ground clearance and *TI* effects over *TSR* to find optimal operating conditions for harvesting maximum power. Physical interpretation and modeling of such complex flow fields require accurate numerical setup for obtaining reliable solutions. Studies previously performed by Rezaeiha et al. [45,46], Franchina et al. [47], and Jiao et al. [48] presents guidelines for accurate CFD modeling and discusses modeling obstacles encountered during simulating flow past a VAWT. We use the aforementioned studies and performed high fidelity CFD simulation using Sliding Mesh Interface (SMI) technique to model rotating turbines in the present work. Simulations have been performed using commercially available multiphysics toolbox ANSYS 19.2. The results show a performance loss of 30.10%, 20.65%, 10.65% at turbine clearance heights of 1.0c, 2.5c, 4.0c respectively. The height of 7.5c yield higher and more consistent performance under given operating conditions. The induced turbulence results identify a decrease in the performance up to 45.42% corresponding to 25% *TI* level.

The distribution of the article is as follows: Section 2 presents the background and definitions of the essential parameters, followed by the geometrical/computational model and solver setup in Section 3. In Section 3.3, we numerically verify the accuracy of solutions using grid/time independence tests and benchmark the results against Howell et al. [49] experimental/numerical data. Parametric study on effects of ground clearance, *TI* variation and selection of optimal *TSR* is discussed in Section 4.

2. Theory and background

2.1. Definition of main parameters

For a given turbine, torque ripple, overall torque and C_p provide a measure of turbines performance. Torque ripple refers to the torque produced by a single turbine blade over a rotation. The net torque represents the cumulative torque magnitude contributions of all the blades. The $C_p$is a ratio of the percentage of power extracted by a turbine to total power available in the wind and provide a direct measure of turbines efficiency. The analytic expression for $C_p$is defined as follows

$$C_p = \frac{P_T}{P_W}, \tag{1}$$

where $P_T = T\omega \times n$is power extracted by the VAWT, and $P_w = \frac{1}{2}A_s V_w^3$is power available in wind.

TSR is another critical parameter used for the classification of turbine operating conditions. It is expressed as the ratio of the rotational speed of the blade's tip to actual wind velocity (V_w), i.e., $TSR = R\omega/V_w$. The performance of SB–VAWT strongly depends on the operating *TSR*. Optimum *TSR* generally depends on the type and configuration of the given wind turbine. For example, a Darrieus

type wind turbine performs efficiently at higher *TSR* in comparison to Savonius type which works optimally for *TSR* lower than unity (i.e., it cannot spin faster than the wind speed). Therefore, an optimal selection of *TSR* is critical for a turbine to extract optimal power from oncoming wind stream.

2.2. Governing equations

Generally, high fidelity studies conducted in the past to simulate flow around SB–VAWT employ either Large Eddy Simulation (LES) [50] or the Unsteady Reynolds–Averaged Navier–Stokes (URANS) [32,51]. The choice of CFD modeling technique mainly depends on the scale of wind turbine simulation and available computational resources. The present work adopt URANS approach, given Mach number ($Ma = \boldsymbol{u}_{Rel}/\boldsymbol{u}_{sound}$, where $\boldsymbol{u}_{Rel}$is the relative velocity and $\boldsymbol{u}_{sound}$is the speed of sound in the fluid) considerations fall under 0.3 for present problem [43,52].

We have solved following two equations for conservation of mass and momentum

$$\frac{\partial \boldsymbol{u}}{\partial t} + \nabla \cdot \left((\boldsymbol{u} - \boldsymbol{u}_g) \otimes \boldsymbol{u}\right) + \nabla \cdot (\nu + \nu_t)\nabla \cdot \left(\boldsymbol{u} + \nabla \boldsymbol{u}^T\right) - \nabla \boldsymbol{p} = \boldsymbol{f}, \tag{2}$$

$$\nabla \cdot \left(\boldsymbol{u} - \boldsymbol{u}_g\right) = 0, \tag{3}$$

here $\boldsymbol{u}$is the fluid velocity, $\boldsymbol{u}_g$grid velocity (zero for the static part of grid), $\boldsymbol{p}$ the fluid pressure, $\boldsymbol{f}$ the applied volume forces, ν and ν_t the fluid viscosity and turbulent eddy–viscosity, respectively.

For turbulence modeling and closure of governing URANS equations $k-\varepsilon$ turbulence model is adopted. The choice of the model is motivated from studies [32,51,53] where the model perform adequately for external and rotating flow simulations. Three variants of $k-\varepsilon$ model are tested - Standard, RNG and Realizable. Each form has similar transport equations for k and ε with slight differences in the way turbulent viscosity and generation/destruction terms are calculated [54]. The equations for $k-\varepsilon$ are defined as

$$\frac{\partial k}{\partial t} + \nabla \cdot (\boldsymbol{u} \otimes k) = \tau_{ij}\nabla \boldsymbol{u} + \nabla \cdot \left[\frac{\nu + \nu_t}{\sigma_k}\right]\nabla\left(k + (\nabla k)^T\right) - \omega k, \tag{4}$$

$$\frac{\partial \varepsilon}{\partial t} + \nabla \cdot (\boldsymbol{u} \otimes \varepsilon) = C_{\varepsilon 1}\frac{\varepsilon}{k}\tau_{ij}\nabla \boldsymbol{u} + \nabla \cdot \left[\frac{\nu + \nu_t}{\sigma_\varepsilon}\right]\nabla\left(\varepsilon + (\nabla \varepsilon)^T\right) - C_{\varepsilon 2}\frac{\varepsilon^2}{k}. \tag{5}$$

For the closure of turbulence quantities, $\nu + \nu_t$accounts for turbulent stresses resulting from Reynolds averaging modeled with $k-\varepsilon$, $\sigma_k/\sigma_\varepsilon$ are turbulent Prandtl numbers for k/ε, and $C_{\varepsilon i}$ for $i = 1, 2$ are the constants of the model.

2.3. Induced turbulence intensities (TI)

Wind condition in a complex urban neighborhood - especially in proximity to high rise buildings, develop into a highly turbulent stream due to bluff body effects (recirculation zones, vorticity). According to the International Electrotechnical Commission (IEC) Standard 64400, turbines should not be operated in winds having turbulent content greater than 16 – 18% for longer periods. However, it is evident from Ledo et al. [19] investigation that *TI* levels can easily rise to 20% in the wake of high rise buildings. Therefore, it becomes essential to carefully examine the performance of SB–VAWTs exposed to such unstable wind conditions. The turbulence is mainly driven by topographical variations (buildings structure, trees, etc.), scales (local and global), and wind gradients. Four common levels of turbulent flow regime that persist in urban canopy i.e. *TI* of 0%, *TI* of 5%, *TI* of 15% and *TI* of 25% are analyzed to investigate performance of SB–VAWT. *TI* in the flow field is calculated using the following expression

$$TI = \frac{u'}{U}, \text{ where, } u' = \sqrt{\frac{1}{3}\left(u_x^{2'} + u_y^{2'} + u_z^{2'}\right)}, \text{ and } U = \sqrt{\frac{1}{3}\left(\overline{u}_x^2 + \overline{u}_y^2 + \overline{u}_z^2\right)}.$$

Characteristic turbulent flow is composed of a mean wind profile superimposed with a minimal fluctuating component. Herein, the levels analyzed in the present work are discussed.

***TI* of** 0%: This incoming wind condition rarely exist at rooftop sites. Such conditions may develop for a relatively short time for sites under the effect of a few obstacles, neutral thermal gradients, and minimal crosswind effects. The flow field under such conditions is represented by the mean velocity component with no spatial fluctuations. Turbine operation under such regimes experiences smooth horizontal flow. Although idealistic, study of these conditions may provide a possible reference against which other variations of *TI* can be assessed.

***TI* of** 5%: These incoming wind conditions are representative of urban neighborhood rooftop sites characterized by a modest variation of topography (building, trees, etc.) Such regimes offer up to 5% *TI*variation and are indicative of conditions a standard urban rooftop turbine experience during its wide range of operation.

***TI* of** 15%: These flow conditions exist at rooftop sites located in the vicinity of relatively dense topography (building, trees, etc.) offering almost 15% *TI* variation. Such conditions provide large variation in spatial and temporal behavior of flow characteristics and significantly turbine power output.

***TI* of** 25%: The rooftop sites concentrated in a skewed topography (densely populated building, trees, etc.) influenced by recirculation zones or under wake effect of other buildings offer up to *TI* of 25%. Such conditions can pertain even at normal rooftop sites in the rare event of gusts and storms. Turbine operation under such a scenario experience significantly unsteady aerodynamic conditions resulting in large power degradation.

3. Wind turbine model

3.1. Geometric model

The CAD model of fixed–pitch SB–VAWT is shown in Fig. 1. The turbine is comprised of three blades constructed from thick NACA0022 airfoil that provide higher structural strength. The turbine has a diameter (D) of 2.5 m, blade chord length (c) of 0.2 m and a power rating of 1.5 kW [32]. The turbine height is systematically varied (i.e., for chord length c, $h = a \times c$) to obtain an optimum

Parameters	Values
Diameter (D)	2.5 m
Chord length (c)	0.2 m
Blade length (b)	2.5 m
Baseline inlet velocity (U_0)	12.0 m/s
Expected power output	1.5 kW
Blade aspect ratio	10.0

Fig. 1. SB–VAWT: CAD model with corresponding geometric properties of the full turbine.

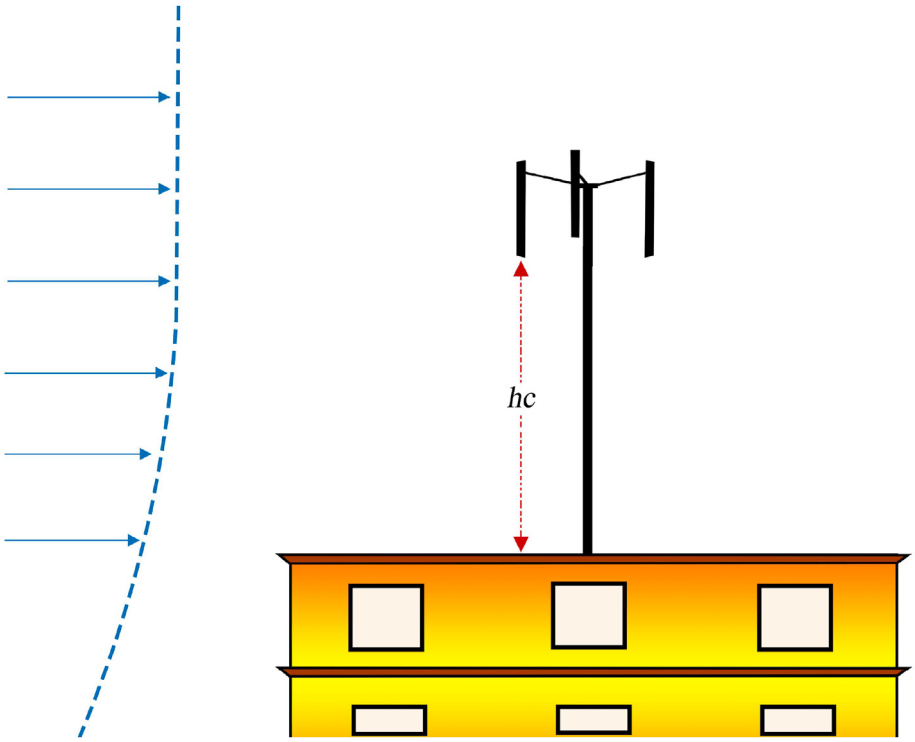

Fig. 2. SB–VAWT: The schematic of turbine placed on a rooftop illustrating variations in height. Five levels of height are considered, i.e. 1.0*c* (Case i), 2.5*c* (Case ii), 4.0*c* (Case iii), 7.5*c* (Case iv), and 10.0*c* (Case v).

clearance height from the ground in section 4. Five cases are considered corresponding to geometric variations in height under fixed *TI*, i.e. $h = 1.0c$ (Case I), $h = 2.5c$ (Case II), $h = 4.0c$ (Case III), $h = 7.5c$ (Case IV) and $h = 10.0c$ (Case V) (see Fig. 2).

3.2. Computational model

Fig. 3, presents schematic of SB–VAWT placed in a 50*c* long and 30*c* wide confined channel that constitutes of stationary boundaries of the computational domain. The coordinate system is located at the center of the turbine, with streamwise direction *x* and cross-stream direction *y*. The geometric model of the turbine is placed inside a cylindrical domain to allow rotation during transient analysis. The two zones are combined through an *interface* boundary condition, which allows the use of a SMI technique to model the rotational effects. Boundary–layer mesh with a progressive ratio of 1.05 is adopted in the vicinity of the blades to capture sharp gradients. The mesh then smoothly transforms into unstructured triangular elements away from the rotor region. Great care is taken to connect the inner and outer mesh regions to allow the correct calculation of fluxes. To ensure the accurate prediction of aerodynamic forces on the blades while keeping the non–dimensional wall-normal distance to $y^+ = 15$, the first cell height is chosen in the range of 1×10^{-4}. This strategy results in the correct calculation of forces without imparting significant requirements on computational resources. The schematic of 2D and

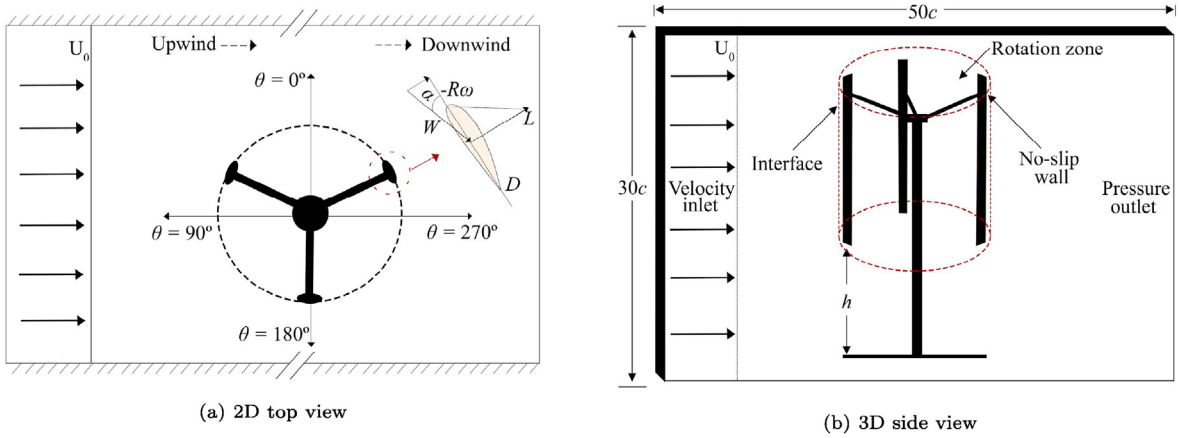

(a) 2D top view

(b) 3D side view

Fig. 3. SB–VAWT: Schematic of turbine placed in a 50clong and 30*c* wide channel. (a) represents the two-dimensional (2D) top view showing the upwind path ($0^\circ \leq \theta \leq 180^\circ$) and downwind path ($180^\circ \leq \theta \leq 360^\circ$) in addition to aerodynamic forces on airfoil during rotation (b) represents the three-dimensional (3D) side view with corresponding boundary conditions.

3D meshes employed in the present work is shown in Fig. 4. For further information on how to select appropriate computational settings and parameters according to previously conducted validation study, the reader is referred to Refs. [42].

3.3. Numerical verification

The numerical accuracy of high fidelity CFD simulations is performed through the grid, time, turbulence model, and spatial discretization independence studies at *TSR* value of 3. The results are verified with the available numerical and experimental data.

3.3.1. Turbulence model

Three variants of $k-\varepsilon$turbulence models are analyzed to ascertain the choice of turbulence model for our numerical study. Fig. 5 (a) show a comparison of computed results using each model in terms of performance prediction. It can be seen that $k-\varepsilon$ standard turbulence model under–predict torque, whereas the RNG and realizable report closer values against experimental values. To highlight underlying differences we plot qualitative representation of contour plots of vorticity magnitudes over a plane as shown in Fig. 5 (b–8). Note that $k-\varepsilon$ realizable results in compact vortices at trailing of each blade, whereas $k-\varepsilon$ standard produces higher *TI* with strong streamline curvature, vortices, and rotation. This stronger turbulence is expected to cause a significant drop in the performance for $k-\varepsilon$ standard turbulence model. We compare the computed average torque and C_p from three turbulence models in Table 1. Given adequate prediction of $k-\varepsilon$ realizable compared to the other two variants, it has been chosen for subsequent simulations in upcoming sections.

3.3.2. Grid and time independence tests

Adequate mesh and time step size are evaluated in both 2D and 3D spatial settings. The number of mesh elements and corresponding torque and C_p are illustrated in Table 2. It can be seen from Fig. 6 (a) that for 2D analysis, mesh size of $78,000$ is reported to provide a mesh independent solution. A coarser grid size of $70,000$ cells under–predicts the torque while a refined mesh size of $86,000$ cells computes a similar solution at the expense of computational cost. For the 3D analysis, Fig. 6 (b)) reports mesh size of 2.2×10^6 suffices in terms of simulation accuracy and computational effort, while lower cells seem to smear down the performance parameters.

To evaluate time step size, we adopted four time steps sizes i.e. $0.0001\ s$, $0.0003\ s$, $0.0005\ s$, $0.0006\ s$. From the analysis, we notice that $0.0005\ s$ provides a time-independent solution. No major difference is reported from 0.0005 to 0.0006. Therefore 0.0005 is used as a time marching step size in present numerical simulations. The time also results in 0.5° azimuthal increment, which, according to the study [46] found to be sufficient. To obtain higher accuracy for temporal and spatial discretization, second-order implicit and second-order upwind schemes are employed as per guidelines presented in Ref. [46].

3.4. Boundary conditions and solver setup

The computational setup containing blade, shafts, and cylindrical hub is imposed with corresponding boundary conditions. The left side of the domain is assigned *velocity inlet* boundary condition. The incoming wind speed is imposed as a fixed mean velocity of $U_0 = 12\ m/s$, while for relevant cases, *TI* levels are induced as described in subsection 2.3. The outlet domain is assigned with a zero pressure gradient. The top and bottom boundaries are assigned as the far–field boundaries with *slip* condition. The turbines' geometrical structure is applied with the *no–slip* boundaries, thereby enabling a realistic zero velocity over turbine structure. The rotor zone, as illustrated in Fig. 3, undergo circular movement corresponding to a rotation angle depending on operating *TSR*. The two outer and inner zones are connected with an *interface* boundary condition. For three–dimensional simulations, *symmetry* boundary conditions are imposed on the upper and lower faces of the computational domain.

`ANSYS Fluent 19.2` multiphysics toolbox is used to conduct parametric numerical simulations. The SIMPLEC scheme is used for the pressure–velocity coupling. Equation (2) and Equation (3) are solved using the density–based solver with Green Gauss Cell–Based scheme for the gradients control and second-order accurate spatial discretization. To handle turbulent conditions, the under–relaxation factors for the turbulent kinetic energy, turbulent dissipation rate, and turbulent viscosity are set at 0.8, 0.8, and 1.0, respectively. The flow field is initialized with the values assigned at the inlet boundary, and the simulations are first solved to obtain a steady–state solution. The solver is then switched to unsteady mode to allow the rotor to move forward at each time–step. The solution obtained from steady–state is used as the baseline solution for unsteady analysis to enable faster convergence and solution blowups. A second-order implicit temporal scheme is used for time marching. The convergence criterion of all flow quantities residuals is set to fall below 1×10^{-5}. Corresponding to the resultant flow velocity vector, the Reynolds number (Re) in present problem ranging from $3\times10^4$to 4×10^5. To avoid laminar to turbulent transition, the flow field is considered fully turbulent.

4. Results and discussion

The performance of urban rooftop SB–VAWT influenced by turbine height, *TI* and *TSR* is investigated in this section.

4.1. Numerical bench–marking

The high fidelity 2D and 3D simulations are benchmarked against experimental and numerical simulations of Howell et al.

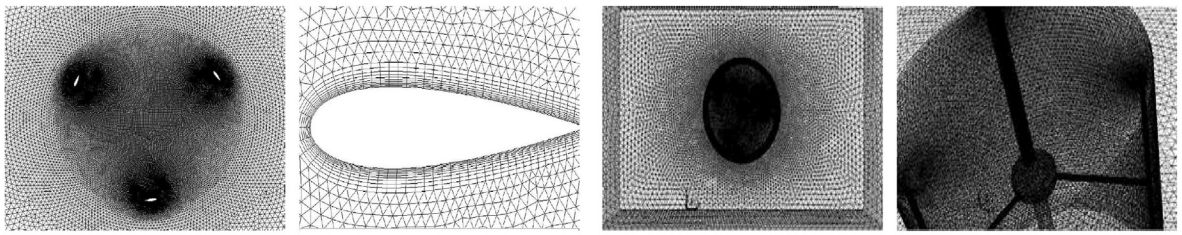

(a) Complete domain $2D$ (b) Zoomed rotor view $2D$ (c) Complete domain $3D$ (d) Zoomed rotor view $3D$

Fig. 4. SB–VAWT: Generated mesh for the two-dimensional (2D) and three-dimensional (3D) models of turbine using Sliding Mesh Interface (SMI).

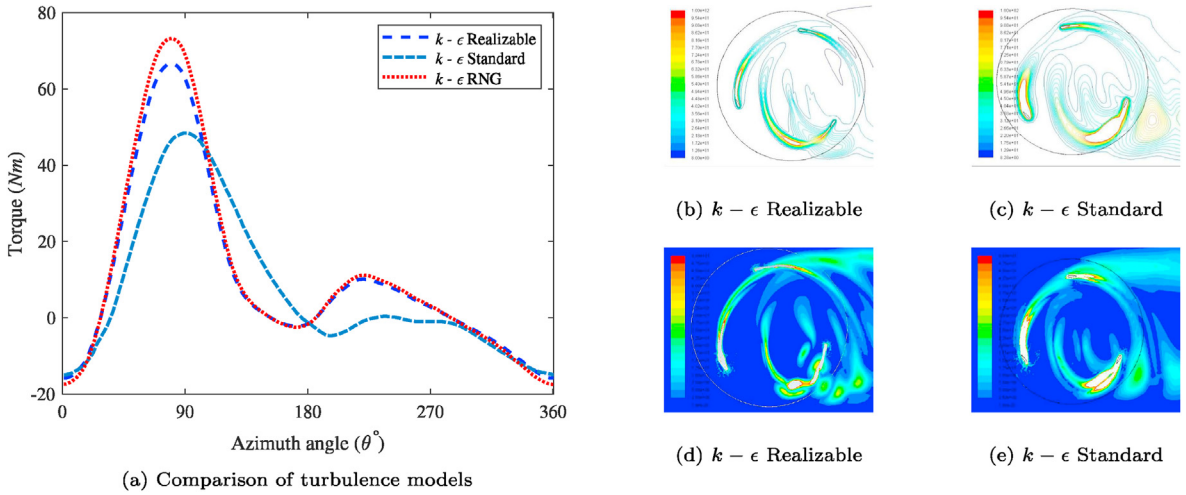

Fig. 5. SB–VAWT: Comparison of $k-\varepsilon$ turbulence models, i.e. Realizable, RNG, and Standard. (a) shows the average torque plotted over one aerofoil rotation while (b), (c) and (d), (e) displays the contour plots for Turbulent Intensity (*TI*) and vorticity magnitudes, respectively.

Table 1
SB–VAWT: Comparison of the $k-\varepsilon$ turbulence models for a laminar flow with *TSR* of 3.0. The values show average torque ($\overline{T}$) and power coefficient (C_p) for one turbine rotation. $k-\varepsilon$ RNG and realizable show close results unlike to the $k-\varepsilon$ standard model.

Turbulence model	$\overline{T}$ (N m)	$\overline{C}_p$
$k-\varepsilon$ Standard	7.85	0.27
$k-\varepsilon$ RNG	11.52	0.32
$k-\varepsilon$ Realizable	10.39	0.31

Table 2
SB–VAWT: Grid independence study for a 2D/3D spatial configuration, indicating effect of grid cells on average torque ($\overline{T}$) and power coefficient (C_p). The optimum grid size for 2D and 3D is computed as 78,000 and 2.2×10^6 gird elements. We notice insignificant variation on the performance coefficients after further increase in grid size.

Grid	Dimension	Size	$\overline{T}(Nm)$	$\overline{C}_p$
1	2D	70,000	5.44	0.437
2	2D	78,000	10.39	0.511
3	2D	86,000	10.67	0.518
4	3D	1.4×10^6	20.46	0.289
5	3D	2.0×10^6	26.52	0.301
6	3D	2.2×10^6	30.95	0.361
7	3D	3.3×10^6	30.47	0.367

[49]. Fig. 7 presents $C_p$plot against *TSRs* at incoming wind speed of 5.07 m/s and C_T for a time period of 1*s*. The experimental measurements used from the literature report an error tolerance value of ±20%, which is included in the form of an error bar in the plots. Note that under high *TSRs* (indicative of low α between the relative wind and rotor blade) present 3D simulations show a good match than Howell et al. [49] which report reduced magnitude of C_p. In general, the present high fidelity 3D simulations accurately predict aerodynamic coefficients and provide a strong basis for the correctness of the present computational setup.

4.2. Effect of ground clearance

Effect of different ground clearances for the urban rooftop SB–VAWT is studied and results are shown for each selected performance parameters. It is important to note that the ground clearance effects are discussed under fixed induced turbulence levels. Five levels are systematically investigated i.e. Case i, Case ii, Case iii, Case iv, Case v corresponding to ground clearance of 1.0*c*, 2.5*c*, 4.0*c*, 7.5*c* and 10.0*c*, respectively. Table 3 depicts the average values of torque, performance coefficients obtained from the high fidelity numerical simulations. The results indicate small changes in the average value of performance coefficient of Case v compared to Case iv i.e. average torque $\overline{T}$of 25.95 *Nm*and $C_p$of 0.367 show a reduction of 25.80 and 0.361 respectively. This represents an overall variation of approximately 0.5%. For the Case iii, a drastic reduction in performance of 10% is reported with corresponding average torque $\overline{T}$of 23.05 *Nm*and $C_p$of 0.352. The magnitudes are indicative of strong performance deterioration due to shear affects arising between blade and ground surface. Note that, Case i and Case ii reports reduction of almost two to three times compared to Case iii. This also show that the corresponding $C_p$values approach 0.341 and 0.328 for each case.Whereas, the results of average torque and $C_p$reports highest magnitudes for Case V, while small va7.5criation are observed between Case v and Case iv i.e. turbine height of 10.0cand 7.5*c*. However, Case iii, Case ii and Case i predicts a reduction of approximately 10.65%, 20.65%and 30.10%respectively. Fig. 10 illustrates the comparison of torque ripple over a single rotation of the turbine. It can be seen that torque ripple over one rotation show a close comparison at ground clearance height of 10.0cand 7.5*c*. Note that, other three heights present a more significant variation in overall magnitude. Fig. 8 and Fig. 9 represents qualitative behavior of flow corresponding to heights of 2.5cand respectively. It is imperative from contours on Plane (A-C) that height of 2.5cresults in greater shear production, especially at lower part of the blade, causing a pressure drops along with power degradation. The flow streamlines remain smooth at 7.5cas seen from contours over Plane (a-f), which show flow is unaffected by lateral shearing effects. These results, in general, are indicative of the fact that turbine mounted at height of 7.5*c* improve average torque and power coefficient.

4.3. Effect of induced turbulent intensity (TI)

The effect of underlying magnitudes of *TIs*, originating from topographical variation, is an urban neighborhood, is discussed in connection to the performance of SB–VAWT. For Case iv, which has been identified as the optimum turbine height level, four levels of *TI* are investigated. The cases - Case iv-1, Case iv-2, Case iv-3, Case iv-4

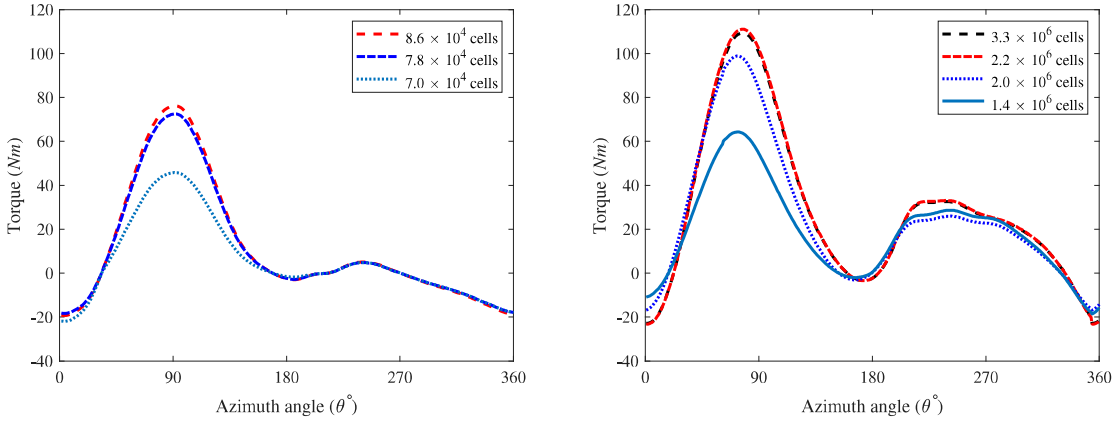

(a) Grid independence study for 2D problem (b) Grid independence study for 3D problem

Fig. 6. SB–VAWT: Grid independence study conducted for 2D (a) and 3D (b) spatial configuration. The results are computed at *TSR* of 3.0.

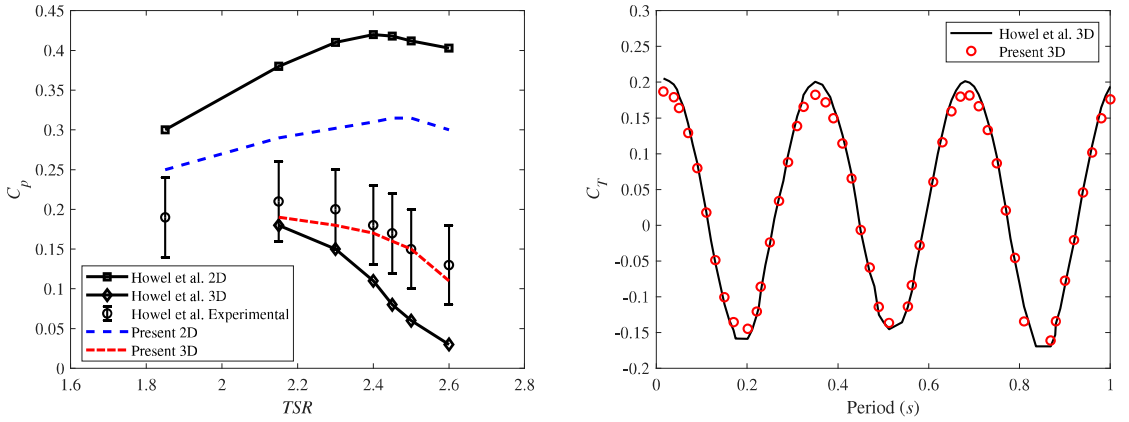

(a) Performance coefficient (C_p) versus TSR (b) Torque coefficient (C_T) for time period 1s at TSR 2.2

Fig. 7. SB–VAWT: Results are benchmarked with Howel et al. [49] experimental and numerical results. Experimental results have been reported at a wind speed of 5.07 m/s. In (a) the present numerical results are within the ±20% error range and more realistic than Howel et al. [49] results at higher *TSR*s. Furthermore, a close agreement with the Howel et al. 3D results is observed in (b), where C_T has been calculated at a *TSR* of 2.2.

Table 3
SB–VAWT: Ground clearance computed at five corresponding heights i.e. Case i: 1.0*c*, Case ii: 2.5*c*, Case iii: 4.0*c*, Case iv: 7.5*c*, Case v: 10.0*c*. Optimal performance is observed corresponding to heights of 7.5*c* and 10.0*c*.

	Ground height (m)	$\overline{T}(Nm)$	% Drop $\overline{T}$	$\overline{C}_p$
Case i	1.0c	18.01	30.10	0.328
Case ii	2.5c	20.47	20.65	0.341
Case iii	4.0c	23.05	10.65	0.352
Case iv	7.5c	25.80	0	0.361
Case v	10.0c	25.95	0.5	0.367

are analyzed corresponding to turbulent content of 0%, 5%, 15%, 25%respectively. Table 4 shows the corresponding comparison of *TI* on the aerodynamic performance of SB–VAWT in terms of $\overline{T}$ generated and C_p. It can be seen that the highest average torque $\overline{T}$ of 25.80 *Nm* and $C_p$of 0.361 is predicted for Case iv-1. The result indicates that the SB–VAWT harness maximum energy while it operates under laminar conditions. Note that, in comparison to Case iv-1 a sudden drop in $\overline{T}$of 19.72 with a corresponding C_p of 0.311 is reported for Case iv-2: which has only 5% induced turbulence level content. This shows a drastic reduction of 23.57% in the performance of SB–VAWT. The $C_p$further reduces to 0.301 and 0.281 corresponding to Case iv-3 and Case iv-4 respectively. It is interesting to note that this behavior is opposite to the experiments performed by Wekesa et al. [55] who performed a numerical investigation on Savonius type rotor under induced turbulence levels and reported an increase in performance due to inflow turbulence. However, the present study, for a Darrieus type SB–VAWT, shows adverse behavior.

It can be noticed that the performance deterioration of $C_p$and $\overline{T}$is lower corresponding to Case iv-3 and Case iv-4 as compared to Case iv-2 and Case iv-3. To understand the behavior, we plot the torque ripple over one rotation for Case iv-1:4 in Fig. 11. It can be seen that torque magnitudes corresponding to a particular turbulent level is not consistent over the rotation. During the upwind path, we obtain a larger magnitude of torques for flow comprised of low induced turbulence (Case iv-2). The high induced turbulence (Case iv-4) shows a reverse trend during the other half cycle. This result implies a better torque generation for higher turbulent flow. The behavior is ascribed to generation of large blade tip vortices as blade and struts pass through the upwind path. While the blade transverse in the downwind side, it interacts with the large vortices of the upwind path. The strength of vortices depends on the

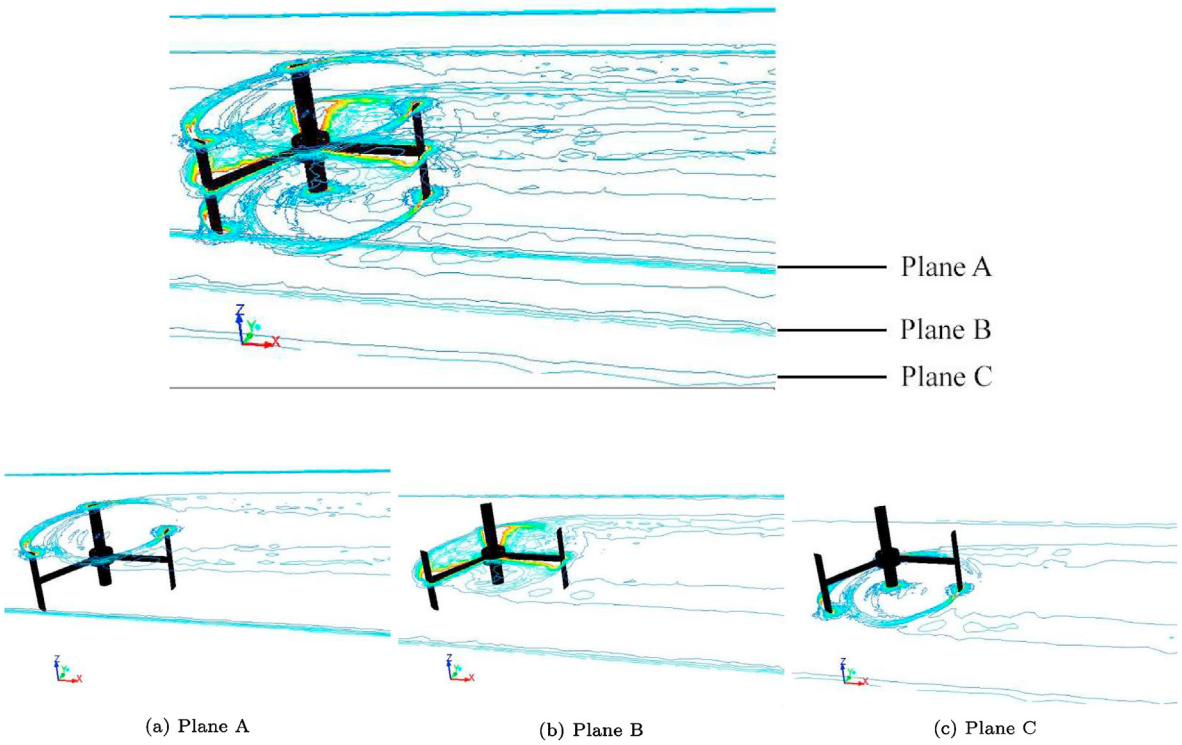

Fig. 8. SB–VAWT: Contours of vorticity on 2D planes while turbine is mounted at 2.5*c* and operating at Tip Speed Ratio (*TSR*) of 3.0.

induced *TI*in the flow, as shown in Fig. 12. Note that, higher turbulent content enhance molecular diffusion, aid to positive momentum exchange among layers and augment overall flow mixing to help wake recover faster. Due to this reason, positive torque magnitudes are observed in downwind paths at high induced turbulence cases (Case iv-4).

4.4. Effect of tip speed ratio (TSR)

TSR directly influence the performance of SB–VAWT on the urban rooftops. Here, the effects of *TSR* on the SB–VAWT for different ground clearance and turbulent intensities are examined. *TSRs* ranging from 1.5 to 4.5 are discussed.

4.4.1. TSR versus height variation

Fig. 13a shows the time-averaged power coefficient C_p calculated at different turbine heights. The spectrum is indicative of the performance of the turbine at a particular *TSR*. The comparison of Case i to Case v for different*TSR* values indicates strong influence of *TSR* on the performance of turbine. A turbine operating at a low value of *TSR* (1.5) produces significantly lower values of $C_p$at given heights. This observation can be attributed to the interdependence of α and characteristic relative flow velocity. At low *TSR* ($1.5 - 2.5$), the α between relative wind velocity and turbine blades is greater than the critical angle of attack (α_{cric}). This causes the turbine to operate in stall mode for a major part during rotation resulting in reduced power generation. For example, at the height of 7.5*c*, the percentage drop in performance for *TSR* values 1.5, 2, and 2.5 are 55.40%, 27.70%, and 5.26%, respectively. In contrast, when the *TSR* is higher ($3.5 - 4.5$), the α becomes lower than the critical value that leads to reduced lift force to contribute effectively towards overall torque magnitude. Moreover, the turbine also starts to spin very fast at such high *TSR* that it creates a blockage for incoming flow. This behavior causes flow streamlines to bypass rotor, which results in reduced performance. The height of 7.5*c*and higher *TSR* ($3.5 - 4.5$) show a percentage drop in performance of 13.85%, 44.32%, and 79.78%, respectively. Meanwhile, *TSR* of 3.0 shows maximum values of C_p at given heights, thereby showing evidence that relative wind maintains α_{cric} throughout upwind and downwind paths resulting in optimum performance.

4.4.2. TSR versus TI

Performance evaluation under range of *TSR* is presented at various *TI* levels. Note that the height of the turbine is remain fixed at to optimal level of 7.5*c*. It can be seen in Fig. 13 (b) that for all cases (Case iv-1 to Case iv-4) maximum values of power coefficient is reported at *TSR* of 3.0. The plots represent a bell-shaped curve, with higher magnitudes shown for lower values of *TSR*. To explain this behavior, we plot Fig. 14 to report magnitudes of torque ripple over single rotation of the turbine blade under fixed ground clearance of 7.5*c*and range of *TSR*. It can be noticed that during the upwind path ($0^\circ \leq \theta \leq 180^\circ$) maximum torque is generated for *TSR* of 4.5; however, this behavior is completely reversed as blade transverse in downwind path ($180^\circ \leq \theta \leq 360^\circ$). The cumulative sum over one rotation ($0^\circ \leq \theta \leq 360^\circ$) produces an overall lower torque magnitude. On the contrary, results for *TSR* of 1.5 indicate good performance in the downwind region. Overall, *TSR* of 3.0 produces optimum values over the entire cycle.

One can also notice that torque magnitudes decrease with increasing induced *TI* for each *TSR*. The reduction appears more significant in the upwind path and a substantial loss in torque magnitudes is observed. We believe that the reason for this behavior is due to variation in effective α for highly turbulent flow, which causes lower magnitudes of aerodynamic coefficients. This, in turn, produces lower contributions to positive torque generation. We notice that the variation becomes less evident and the torque ripple curve begins to converge monotonically at higher *TI* levels.

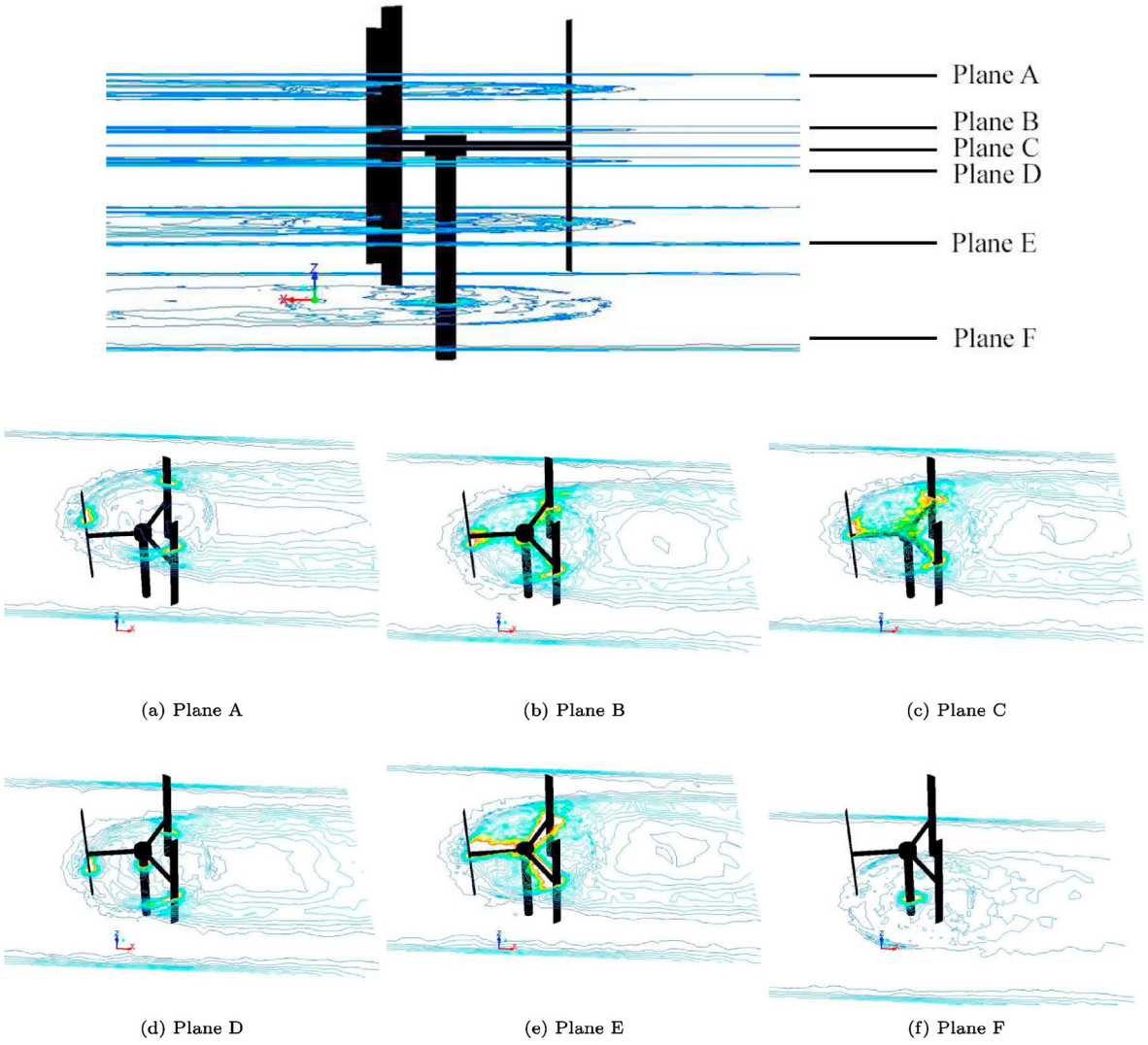

Fig. 9. SB–VAWT: Contours of vorticity on 2D planes while turbine is mounted at 7.5cand operating at Tip Speed Ratio (*TSR*) of 3.0.

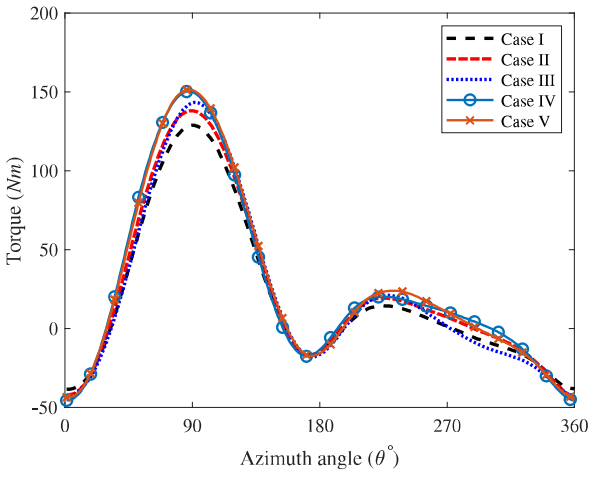

Fig. 10. SB–VAWT: Torque ripple at five corresponding heights i.e. Case i: 1.0*c*, Case ii: 2.5*c*, Case iii: 4.0*c*, Case iv: 7.5*c*, Case v: 10.0*c*. A drop in torque generation is observed at low ground clearances as compared to higher ones.

Table 4
SB–VAWT: Effect of the Turbulent Intensity (*TI*) on the performance of average torque ($\overline{T}$), power coefficient ($\overline{C}_p$) and percentage drop in the performance at four levels i.e., Case iv-1: *TI* of 0%, Case iv-2: *TI* of 5%, Case iv-3: *TI* of 15%, Case iv-4: *TI* of 25%.

	% *TI*	$\overline{T}$ (N m)	% Drop $\overline{T}$	$\overline{C}_p$
Case iv-1	0	25.80	0	0.361
Case iv-2	5	19.72	23.57	0.311
Case iv-3	15	17.16	33.49	0.301
Case iv-4	25	15.68	40.22	0.281

4.5. Remark

As previously proposed in the study [56] performed on the best practice guidelines of turbulence models for VAWT's, the variants of k-ω SST exhibited superior performance for prediction of the wake vortex evolution and dynamic stall. We believe that although k-ε show adequate results in the verification of present study and performed well for the underlying aims and objective of the present work, we still anticipate that the simulation could benefit with the use of k-ω SST variants.

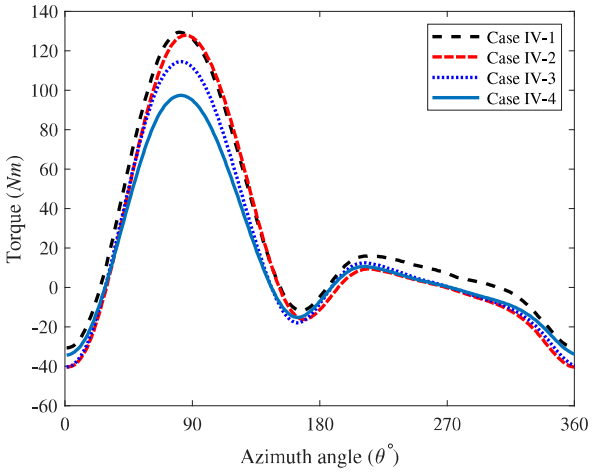

Fig. 11. SB–VAWT: Effect of Turbulent Intensity (*TI*) on the torque generation under four levels i.e., Case iv-1: *TI* of 0%, Case iv-2: *TI* of 5%, Case iv-3: *TI* of 15%, Case iv-4: *TI* of 25%.

5. Conclusion

The performance of rooftop Vertical Axis Wind Turbine (VAWT) was investigated using high fidelity Computational Fluid Fynamics (CFD) simulations. Effect of Tip Speed Ratio (*TSR*), ground clearance and Turbulence Intensity (*TI*) on the performance parameters of power coefficient (C_p) and average torque ($\overline{T}$) were reported. Turbine performance was evaluated under four topographic variations offering, laminar flow (*TI* of 0%), mild (*TI* of 5%), intermediate (*TI* of 15%) and high (*TI* of 25%) turbulent levels. The turbine was also tested under five clearance heights from ground $1.0c$,$2.5c$,$4.0c$,$7.5c$, $10.0c$(where c being chord length of blade and is equivalent to 0.2 m) to compute the optimum height that results minimal shearing effects and yields consistent power under fixed turbulent intensity conditions.

Main conclusions drawn from the work are as follows:

1. The performance of rooftop VAWT can be enhanced by mounting at an optimum height that offers significantly less ground shearing effects. For example, the present turbine at *TSR* of 3.0 and ground clearance of $7.5c$yield maximum efficiency. The optimum performance is ascribed to negligible wind shearing effects at $7.5c$that otherwise have shown to impart complex flow to the turbine itself, resulting in pressure drop and power degradation. Meanwhile, corresponding to height levels of $1.0c, 2.5c, 4.0c$ a reducing of performance of 30.10%, 20.65%, 10.65%, respectively, were observed whereas heights larger than $7.5c$ report a constant value of performance parameters (C_p and $\overline{T}$).
2. The outputs of VAWT installed at rooftops is influenced by topographical conditions of the neighborhood they have been exposed to. For example, for induced turbulence intensities levels of 5%, 15% and 25% resulted in a corresponding drop of approximately 10.0% for C_p and $\overline{T}$. Also, maximum energy for a single blade is harvested in the upwind path, ($0^\circ \leq \theta \leq 180^\circ$). This produce disturbance that travels to the downwind path ($180^\circ \leq \theta \leq 360^\circ$) affecting torque generation. Note that, there was no unique trend observed for TI and $\overline{T}$for Darrieus type

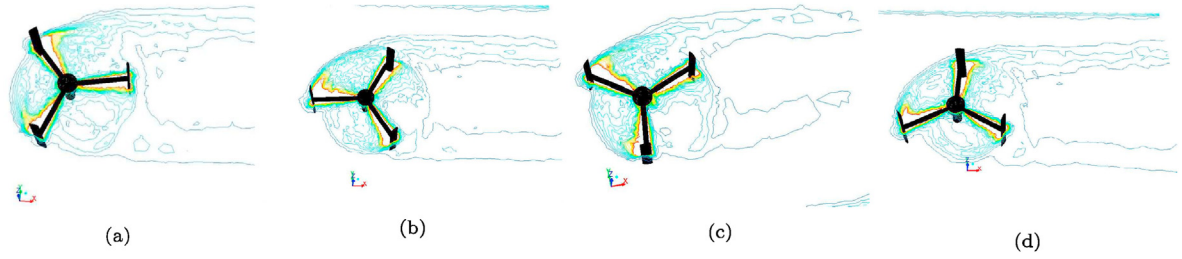

Fig. 12. SB-VAWT: Contours of vorticity corresponding to four Turbulent Intensity *TI* levels: (a) Case iv-1: *TI* of 0%, Case iv-2: *TI* of 5%, Case iv-3: *TI* of 15%, Case iv-4: *TI* of 25%.

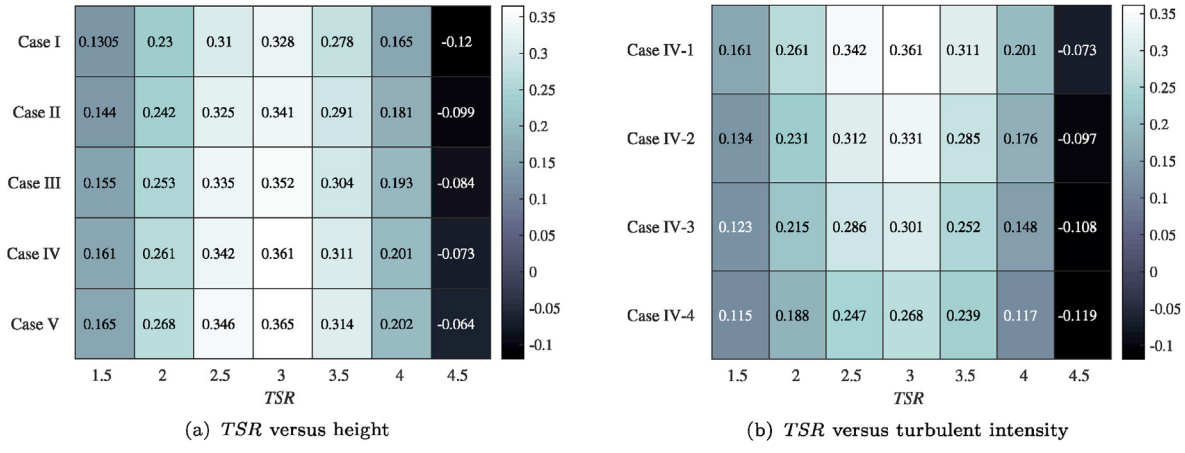

(a) TSR versus height (b) TSR versus turbulent intensity

Fig. 13. SB–VAWT: Effect of *TSR* on the performance of Darrieus type H–VAWT. Figure shows C_p for varying heights (a) and turbulent intensities (b). Optimal performance as been reported for $TSR = 3.0$ and 0%turbulent intensity. Note dark and light color are indicative of the worse and good performance of turbine respectively. (For interpretation of the references to color in this figure legend, the reader is referred to the Web version of this article.)

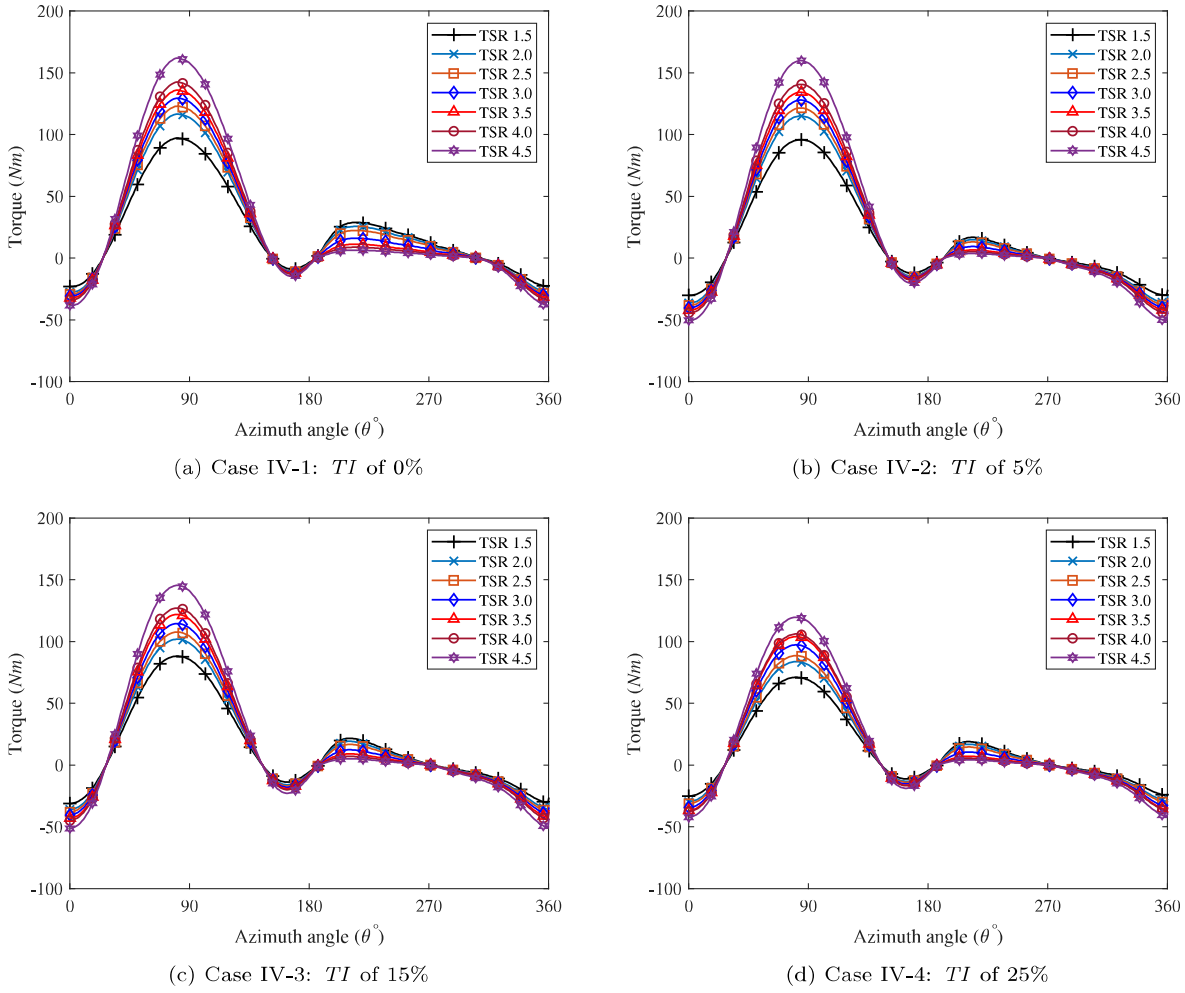

Fig. 14. SB–VAWT: Parametric study under varying Tip Speed Ratio (*TSR*) and Turbulent Intensities (*TI*).

turbine in the downwind path, which is contradictory to the behavior reported by Wekesa et al. [55]; where inflow turbulence produces a direct increase in the performance of Savonious VAWT.

3. In comparison to higher *TSR* (3.5 – 4.5), lower *TSR* (1.5 – 2.5) showed optimal performance at variable turbulent intensity. *TSR* of 3.0 was reported to provide maximum performance with a corresponding $C_p$of 0.361. Another noteworthy observation is that trend resulting from complex topographic variations on torque ripple starts to converge monotonically over the range of *TSR*.

A possible extension of this work is to employ Large Eddy Simulation (LES) technique to evaluate unsteady wind flow characteristic with physical turbine mounted on buildings, whilst the urban neighborhood is incorporated in the full-scale modeling. This modeling strategy enable to simulate exact dynamic conditions of flow in urban dwellings and therefore provide better feasibility of rooftop turbine installations in urban settings.

CRediT authorship contribution statement

M. Salman Siddiqui: Conceptualization, Methodology, Validation, Writing - original draft. **Muhammad Hamza Khalid:** Data curation. **Rizwan Zahoor:** Writing - review & editing. **Fahad Sarfraz Butt:** Writing - review & editing. **Muhammed Saeed:** Writing - review & editing. **Abdul Waheed Badar:** Writing - review & editing.

Declaration of competing interest

The authors declare that they have no known competing financial interests or personal relationships that could have appeared to influence the work reported in this paper.

Acknowledgments

The author are grateful to Imran Akhtar and Naveed Durrani for their valuable suggestions at the beginning of this work. The research was partially supported by Slovenian Grant Agency (ARRS) within Program Group P2-0162.

References

[1] M.S. Siddiqui, A. Rasheed, T. Kvamsdal, Numerical assessment of rans turbulence models for the development of data driven reduced order models, Ocean Eng. 196 (2020), 106799.
[2] World Oil Outlook 2040 (Opec), 2018.
[3] M.M.A. Bhutta, N. Hayat, A.U. Farooq, Z. Ali, S.R. Jamil, Z. Hussain, Vertical axis wind turbine–a review of various configurations and design techniques, Renew. Sustain. Energy Rev. 16 (4) (2012) 1926–1939.
[4] M.S. Siddiqui, A. Rasheed, M. Tabib, T. Kvamsdal, Numerical investigation of modeling frameworks and geometric approximations on NREL 5MW wind turbine, Renew. Energy 132 (2019) 1058–1075.

[5] BP Energy Outlook 2019 Edition, 2019.
[6] M.S. Siddiqui, T. Kvamsdal, A. Rasheed, High fidelity computational fluid dynamics assessment of wind tunnel turbine test, J. Phys. Conf. 1356 (2019), 012044.
[7] A. Barnes, B. Hughes, Determining the impact of VAWT farm configurations on power output, Renew. Energy 143 (2019) 1111–1120.
[8] M.S. Siddiqui, S.T.M. Latif, M. Saeed, M. Rahman, A.W. Badar, S.M. Hasan, Reduced order model of offshore wind turbine wake by proper orthogonal decomposition, Int. J. Heat Fluid Flow 82 (2020), 108554.
[9] H. Peng, Z. Han, H. Liu, K. Lin, H. Lam, Assessment and optimization of the power performance of twin vertical axis wind turbines via numerical simulations, Renew. Energy 147 (2020) 43–54.
[10] M.Z. Shiraz, A. Dilimulati, M. Paraschivoiu, Wind power potential assessment of roof mounted wind turbines in cities, Sustain. Cities Soc. 53 (2020), 101905.
[11] M.S. Siddiqui, A. Rasheed, T. Kvamsdal, Validation of the numerical simulations of flow around a scaled-down turbine using experimental data from wind tunnel, Wind Struct. 29 (6) (2019) 405–416.
[12] S. Eriksson, H. Bernhoff, M. Leijon, Evaluation of different turbine concepts for wind power, Renew. Sustain. Energy Rev. 12 (5) (2008) 1419–1434.
[13] A.-S. Yang, Y.-M. Su, C.-Y. Wen, Y.-H. Juan, W.-S. Wang, C.-H. Cheng, Estimation of wind power generation in dense urban area, Appl. Energy 171 (2016) 213–230.
[14] L.C. Pagnini, M. Burlando, M.P. Repetto, Experimental power curve of small-size wind turbines in turbulent urban environment, Appl. Energy 154 (2015) 112–121.
[15] D.G.J. Marie, Turbine Having its Rotating Shaft Transverse to the Flow of the Current, Dec. 8 1931. US Patent 1,835,018.
[16] S. Li, Y. Li, C. Yang, X. Zheng, Q. Wang, Y. Wang, D. Li, W. Hu, Experimental and numerical investigation of the influence of roughness and turbulence on lut airfoil performance, Acta Mech. Sin. 35 (6) (2019) 1178–1190.
[17] L. Du, G. Ingram, R.G. Dominy, A review of h-darrieus wind turbine aerodynamic research, Proc. IME C J. Mech. Eng. Sci. 233 (23–24) (2019) 7590–7616.
[18] M.A. Heath, J.D. Walshe, S.J. Watson, Estimating the potential yield of small building-mounted wind turbines, Wind Energy: Int. J. Progr. Appl. Wind Power Convers. Technol. 10 (3) (2007) 271–287.
[19] L. Ledo, P. Kosasih, P. Cooper, Roof mounting site analysis for micro-wind turbines, Renew. Energy 36 (5) (2011) 1379–1391.
[20] F. Balduzzi, A. Bianchini, E.A. Carnevale, L. Ferrari, S. Magnani, Feasibility analysis of a darrieus vertical-axis wind turbine installation in the rooftop of a building, Appl. Energy 97 (2012) 921–929.
[21] K. Anup, J. Whale, S.P. Evans, P.D. Clausen, An investigation of the impact of wind speed and turbulence on small wind turbine operation and fatigue loads, Renew. Energy 146 (2019) 87–98.
[22] S. Rafailidis, Influence of building areal density and roof shape on the wind characteristics above a town, Boundary-Layer Meteorol. 85 (2) (1997) 255–271.
[23] S. Hassanli, S.A. Jafari, K.C. Kwok, Flow enhancement in tall buildings for wind energy generation, in: 8th International Colloquium on Bluff Body Aerodynamics and Applications, Northeastern University, Boston, Massachusetts, USA, 2016. June 7-11.
[24] B. Blocken, J. Carmeliet, T. Stathopoulos, CFD evaluation of wind speed conditions in passages between parallel buildings—effect of wall-function roughness modifications for the atmospheric boundary layer flow, J. Wind Eng. Ind. Aerod. 95 (9–11) (2007) 941–962.
[25] H. Bai, C. Chan, X. Zhu, K. Li, A numerical study on the performance of a savonius-type vertical-axis wind turbine in a confined long channel, Renew. Energy 139 (2019) 102–109.
[26] C.S. Ferreira, B. Geurts, Aerofoil optimization for vertical-axis wind turbines, Wind Energy 18 (8) (2015) 1371–1385.
[27] G. Bedon, S. De Betta, E. Benini, Performance-optimized airfoil for darrieus wind turbines, Renew. Energy 94 (2016) 328–340.
[28] P.-L. Delafin, T. Nishino, L. Wang, A. Kolios, Effect of the number of blades and solidity on the performance of a vertical axis wind turbine, in: Journal of Physics: Conference Series, vol. 753, IOP Publishing, 2016, 022033.
[29] Z. Cheng, H.A. Madsen, Z. Gao, T. Moan, Effect of the number of blades on the dynamics of floating straight-bladed vertical axis wind turbines, Renew. Energy 101 (2017) 1285–1298.
[30] A. Rezaeiha, I. Kalkman, B. Blocken, Effect of pitch angle on power performance and aerodynamics of a vertical axis wind turbine, Appl. Energy 197 (2017) 132–150.
[31] A. Rezaeiha, I. Kalkman, H. Montazeri, B. Blocken, Effect of the shaft on the aerodynamic performance of urban vertical axis wind turbines, Energy Convers. Manag. 149 (2017) 616–630.
[32] M. Siddiqui, N. Durrani, I. Akhtar, Quantification of the effects of geometric approximations on the performance of a vertical axis wind turbine, Renew. Energy 74 (2015) 661–670.
[33] J. Cace, R. ter Horst, H. Syngellakis, I. Power, Urban wind turbines, Guidelines for small wind turbines in the built environment, Article online, www.urban-wind.org, 2007, 1–41.
[34] A. Glass, G. Levermore, Micro wind turbine performance under real weather conditions in urban environment, Build. Serv. Eng. Technol. 32 (3) (2011) 245–262.
[35] M. Dowley, A Successful Roof-Top Wind Power Project?, Ph.D. thesis Murdoch University, 2010.
[36] I. AWS Scientific, N. R. E. L. (US), Wind Resource Assessment Handbook: Fundamentals for Conducting a Successful Monitoring Program, The Laboratory, 1997.
[37] F. Emejeamara, A. Tomlin, A Method for Estimating the Potential Power Available to Building Mounted Wind Turbines within Turbulent Urban Air Flows, Renewable Energy.
[38] S. Wang, Y. Zhou, M.M. Alam, H. Yang, Turbulent intensity and Reynolds number effects on an airfoil at low Reynolds numbers, Phys. Fluids 26 (11) (2014), 115107.
[39] K. Sunderland, T. Woolmington, J. Blackledge, M. Conlon, Small wind turbines in turbulent (urban) environments: a consideration of normal and weibull distributions for power prediction, J. Wind Eng. Ind. Aerod. 121 (2013) 70–81.
[40] A.C. Molina, T. De Troyer, T. Massai, A. Vergaerde, M.C. Runacres, G. Bartoli, Effect of turbulence on the performance of VAWTs: an experimental study in two different wind tunnels, J. Wind Eng. Ind. Aerod. 193 (2019), 103969.
[41] K.-Y. Lee, S.-H. Tsao, C.-W. Tzeng, H.-J. Lin, Influence of the vertical wind and wind direction on the power output of a small vertical-axis wind turbine installed on the rooftop of a building, Appl. Energy 209 (2018) 383–391.
[42] A. Rezaeiha, H. Montazeri, B. Blocken, Characterization of aerodynamic performance of vertical axis wind turbines: impact of operational parameters, Energy Convers. Manag. 169 (2018) 45–77.
[43] M.S. Siddiqui, A. Rasheed, T. Kvamsdal, M. Tabib, Effect of turbulence intensity on the performance of an offshore vertical axis wind turbine, Energy Procedia 80 (2015) 312–320.
[44] A. Posa, Influence of tip speed ratio on wake features of a vertical axis wind turbine, J. Wind Eng. Ind. Aerod. 197 (2020), 104076.
[45] A. Rezaeiha, H. Montazeri, B. Blocken, CFD analysis of dynamic stall on vertical axis wind turbines using scale-adaptive simulation (sas): comparison against urans and hybrid RANS/LES, Energy Convers. Manag. 196 (2019) 1282–1298.
[46] A. Rezaeiha, H. Montazeri, B. Blocken, Towards accurate CFD simulations of vertical axis wind turbines at different tip speed ratios and solidities: guidelines for azimuthal increment, domain size and convergence, Energy Convers. Manag. 156 (2018) 301–316.
[47] N. Franchina, G. Persico, M. Savini, 2d-3d computations of a vertical axis wind turbine flow field: modeling issues and physical interpretations, Renew. Energy 136 (2019) 1170–1189.
[48] J. He, X. Jin, S. Xie, L. Cao, Y. Wang, Y. Lin, N. Wang, Cfd modeling of varying complexity for aerodynamic analysis of h-vertical axis wind turbines, Renew. Energy 145 (2020) 2658–2670.
[49] R. Howell, N. Qin, J. Edwards, N. Durrani, Wind tunnel and numerical study of a small vertical axis wind turbine, Renew. Energy 35 (2) (2010) 412–422.
[50] T. Uchida, Y. Ohya, Micro-siting technique for wind turbine generators by using large-eddy simulation, J. Wind Eng. Ind. Aerod. 96 (10–11) (2008) 2121–2138.
[51] M.S. Siddiqui, N. Durrani, I. Akhtar, Numerical study to quantify the effects of struts and central hub on the performance of a three dimensional vertical axis wind turbine using sliding mesh, in: ASME 2013 Power Conference, American Society of Mechanical Engineers, 2013. V002T09A020–V002T09A020.
[52] M.S. Siddiqui, E. Fonn, T. Kvamsdal, A. Rasheed, Finite-volume high-fidelity simulation combined with finite-element-based reduced-order modeling of incompressible flow problems, Energies 12 (7) (2019) 1271.
[53] C. Simao Ferreira, G. van Bussel, G. Van Kuik, 2D CFD simulation of dynamic stall on a vertical axis wind turbine: verification and validation with PIV measurements, 1367, in: 45th AIAA Aerospace Sciences Meeting and Exhibit, 2007.
[54] A. F. U. Guide, Release 19.0, Ansys Inc.
[55] D.W. Wekesa, C. Wang, Y. Wei, W. Zhu, Experimental and numerical study of turbulence effect on aerodynamic performance of a small-scale vertical axis wind turbine, J. Wind Eng. Ind. Aerod. 157 (2016) 1–14.
[56] A. Rezaeiha, H. Montazeri, B. Blocken, On the accuracy of turbulence models for CFD simulations of vertical axis wind turbines, Energy 180 (2019) 838–857.